

Fe₃O₄-TiO₂/chitosan nanobiocomposite as a novel cadmium adsorbent: fabrication, characterization, equilibrium isotherms, adsorption kinetics, and thermodynamics study

A. Sadeghi^a, H. Tashakkorian^{b,*}, A.R. Abri^a, M. Tajbakhsh^c

^aChemistry Department, Azarbaijan Shahid Madani University, 53714-161 Tabriz, Iran, emails: ali.sadeghirad@yahoo.com (A. Sadeghi), Ar.abri@yahoo.com (A.R. Abri)

^bCellular and Molecular Biology Research Center (CMBRC), Health Research Institute, Babol University of Medical Sciences, Babol 47176 41367, Iran, email: H.Tashakkorian@gmail.com

^cFaculty of chemistry, Mazandran University, Babolsar 47415, Iran, email: mahmood.tajbakhsh32@gmail.com

Received 1 May 2018; Received 24 September 2018

ABSTRACT

A new magnetic nanocomposite (MNC) was prepared by grafting 3-chloropropyltrimethoxysilane and melamine (CPMSi-Mel) onto the surface of Fe₃O₄@TiO₂ nanoparticles. Then, nanocomposite of chloroacetyl-chitosan (CACS) and (Fe₃O₄@TiO₂-CPMSi-Mel) was fabricated from coprecipitation of CACS on the (Fe₃O₄@TiO₂-CPMSi-Mel) nanoparticles. The synthesized MNC was characterized by Fourier transform infrared spectroscopy, X-ray diffraction analysis, field emission scanning electron microscopy, transmission electron microscopy, CHN elemental analysis, thermogravimetric analysis, and vibrating sample magnetometer. The ability of MNC for removing heavy metal ion (Cd²⁺) from polluted water was studied, and the effects of different parameters on the adsorption characteristics were investigated. The adsorption equilibrium data were well explained by the Langmuir isotherm model. The sorption kinetics was tested with pseudo-first-order and pseudo-second-order reaction and the rate constants of kinetic models were calculated. Results indicate that Cd²⁺ uptake process followed the pseudo-second-order rate expression. Furthermore, thermodynamic studies specify that adsorption was spontaneous and endothermic. The adsorption mechanism onto MNC was controlled by electrostatic attraction between MNC and Cd²⁺. Excellent adsorption capacity with other advantages such as reusability, easy separation, and environment-friendly composition make them suitable adsorbents for removal of heavy metal ions from environmental and industrial wastes.

Keyword: Nanocomposite; Magnetic nanoparticles; Chitosan; Cadmium removal; Adsorption equilibrium data; Sorption kinetics; Thermodynamic parameters

1. Introduction

Heavy metals as trace amount are essential for the body and must be supplied in the diet. However, most of them are toxic in certain chemical forms at high dose. Among them, from environmental point of view cadmium, mercury, and lead are potentially toxic even at low concentration [1,2]. Cadmium has been used for many years as an agent in electroplating, coating, and a pigment in the industry. In recent

years, cadmium consumption is mainly limited to rechargeable nickel-cadmium batteries for reason of its adverse health effects [3–5]. While heavy metals occur naturally on Earth, the main contribution of environmental pollution comes from the anthropogenic sources including mining, metal smelting, industrial effluents, solid and liquid waste disposal, agriculture, and atmospheric deposition. Unfortunately, unlike organic pollution, heavy metal persist indefinitely in the environment and cannot be destroyed or degraded. Therefore, a variety of methods has been proposed for heavy metals pollution treatment, such as adsorption, chemical precipitation [6],

* Corresponding author.

osmosis [7], and cation-exchange [8]. Biosorption, as a passive adsorption, offers an effective, convenient, and low cost way for the removal of a wide range of metallic pollutions in environmental remediation [9–11]. Chitosan is excellent biosorbent in treatment technologies due to the presence of high number of hydroxyl and amino groups in its polymeric structure, which makes it suitable candidate for metal ions recovery [12,13]. The adsorption properties of chitosan are a function of the degree of deacetylation in its manufacturing process, the type of the metal ion, and the pH. Chemical modification and group functionalization are key issues to increase the adsorption capacity, selectivity, and synthesis of new chitosan analogues [14,15]. Magnetic chitosan nanocomposites have attracted a great deal of attention due to their unique properties, which combines easily separation from the solution by magnetic field, and enhancement of the sorption capability using functionalized biopolymer [16–18]. Various magnetic composites of chitosan have been applied as adsorbent matrix in wastewater treatment. For example, magnetic composites using poly(vinyl alcohol) and chitosan were fabricated to employ as dye remover [19]. A modified magnetic resin was prepared by grafting Schiff base of thiourea and glutaraldehyde on the surface of chitosan to increase selective adsorption of mercury(II) ions. [20] These category of studies demonstrate that the combination of the high adsorption properties of biopolymer such as chitosan derivatives with magnetic properties of magnetic nanomaterials result in new functional structures, which can be effectively utilized for treatment of toxic metal pollutions with the lowest impact on the environment [21,22]. In extension to our previous studies in the field of synthesis of novel structures with reliable sorption potential, herein, the preparation of an effective magnetic multicomponent nanoadsorbent for removal of cadmium ion and exploration of its characteristics were surveyed [23–25]. The adsorption of Cd(II) on the nanocomposite was studied in different conditions of treatment time, temperature, adsorbent dosage, and pH of solution. Different isotherm models were applied to experimental data for characterization of adsorption equilibrium isotherm. Moreover, the adsorption kinetics was modeled from experiments and the related mechanisms were proposed.

2. Materials and methods

2.1. Materials

$\text{FeCl}_2 \cdot 4\text{H}_2\text{O}$ and $\text{FeCl}_3 \cdot 6\text{H}_2\text{O}$ (Sigma-Aldrich) were used as received for magnetic particle synthesis. Ammonium hydroxide (25wt%), chitosan, (CS, molecular weight = 1,100 kDa, deacetylation degree 75%) titanium(IV) oxide, *N*-methylpyrrolidone (NMP), chloroacetyl chloride (CAC), 3-chloropropyltrimethoxysilane (CPMSi), cadmium chloride, and melamine (Mel) were all purchased from Sigma-Aldrich Company (Germany). Potassium carbonate, potassium iodide, sodium hydroxide, methanol, dimethylsulfoxide (DMSO), *N,N*-dimethylformamide (DMF), diethyl ether, and acetone were obtained from Merck company (Darmstadt, Germany).

2.2. Preparation of chloroacetyl-chitosan

Chitosan (1 g) was dissolved into NMP (45 mL) under bubbling argon gas. After reducing temperature of solution

to 0°C, chloroacetyl chloride (5.9 mL, 75 mmol) in NMP (5 mL) was added. Mixed solution was stirred for 15 min and 3 h at 0°C and room temperature, respectively. The polymer synthesized (named as chloroacetyl-chitosan (CACS)) was precipitated from solution by addition of diethyl ether. After filtration, CACS was rinsed twice with diethyl ether (20 mL) and methanol (20 mL), and then dried under vacuum condition [26].

2.3. Preparation of magnetic $\text{Fe}_3\text{O}_4@/\text{TiO}_2$ nanoparticles

Coprecipitation method of Bo et al. [27] was used with some modification for synthesis of magnetic nanoparticles. $\text{FeCl}_3 \cdot 6\text{H}_2\text{O}$ (2 g, 7.32 mmol) and $\text{FeCl}_2 \cdot 4\text{H}_2\text{O}$ (0.73 g, 2.70 mmol) were added to a flask containing TiO_2 (1 g, 12.53 mmol) and distilled water (35 mL). Solution was thermostat at 85°C and vigorously stirred for 30 min under bubbling nitrogen gas. Magnetic nanoparticles were immediately obtained in form of black solids by addition of ammonia (25%, 4 mL) to the solution. The nanoparticles produced were washed three times with water, and then one time with acetone. Nanoparticles was gathered by magnetic filtration, dried for half of a day at 45°C, and then stored in the vacuum desiccator.

2.4. Surface modification of $\text{Fe}_3\text{O}_4@/\text{TiO}_2$ nanoparticles

$\text{Fe}_3\text{O}_4@/\text{TiO}_2$ (2 g) was sonicated in dry toluene (40 mL) for 30 min. After addition of 3-chloropropyltrimethoxysilane (1 mL), solution was agitated for a day at 90°C under bubbling argon. Silanized nanoparticles ($\text{Fe}_3\text{O}_4@/\text{TiO}_2\text{-CPMSi}$) were magnetically separated and then washed twice with ethanol (20 mL). The nanoparticles prepared (0.5 g) were added to a flask containing a stirred solution of dry DMSO (20 mL), potassium carbonate (0.5 g, 3 mmol), melamine (0.25 g, 1 mmol), and potassium iodide (0.6 g, 3 mmol). The flask was kept for 3 d at 90°C. The functionalized nanoparticles ($\text{Fe}_3\text{O}_4@/\text{TiO}_2\text{-CPMSi-Mel}$) were removed from the solution by magnetic filtration, washed twice with ethanol (20 mL), and then dried for a day at 50°C in a vacuum oven.

2.5. Preparation of $\text{Fe}_3\text{O}_4@/\text{TiO}_2\text{-CPMSi-Mel-CACS}$ composite

In a Erlenmeyer flask, $\text{Fe}_3\text{O}_4@/\text{TiO}_2\text{-CPMSi-Mel}$ (0.2 g) and CACS (0.8 g) were added to DMF (20 mL). The reaction was catalyzed by potassium carbonate under bubbling of argon and stirring at 80°C for 1 d. After cooling to room temperature, nanocomposites ($\text{Fe}_3\text{O}_4@/\text{TiO}_2\text{-CPMSi-Mel-CACS}$) were removed from the solution by magnetic filtration, washed several times with deionized water and twice with acetone (10 mL), and then dried for a day at 50°C in a vacuum oven.

2.6. Characterization methods

Fourier transform infrared (FT-IR) spectroscopy of the sample was obtained on a Bruker Tensor 27 spectrometer (Bruker, Karlsruhe, Germany). X-ray diffraction (XRD) analysis of nanocomposite was recorded at 25°C on a RigakuD/Max-2550 powder diffractometer (XRD, Shibuya-ku, Tokyo, Japan). Field emission scanning electron microscope (FESEM) was recorded on a Hitachi S4160 instrument (Tokyo,

Japan). Transmission electron microscopy (TEM) analyses were done using a TEM microscope (Philips CM120). Thermogravimetric analysis (TGA) was performed on LENSES STAPT-1000 calorimeter (Linseis STA PT1000, Selb, Germany) under nitrogen gas by scanning at the heating speed of 10°C/min up to 900°C. Vibrating sample magnetometer (VSM) was supplied by Daghigh Kavir Corporation (Kashan, Iran).

2.7. Adsorption measurement

The effect of sorbent dosage, initial concentration of cadmium ion, contact time, pH, and temperature was studied on adsorption properties of nanocomposite in a series of batch experiments. For this purpose, adsorption experiments were conducted in flasks containing 50 mL solution of nanocomposite (5–100 mg) with a known initial cadmium ion concentration (10–100 mg/L) at constant pH value (in the range of 3–10) and for temperatures of 25°C–45°C. The initial and final Cd²⁺ concentration was determined by an atomic adsorption spectrophotometer (Hewlett-Packard 3510, NovAA-400, Analytic jena AG, Jena, Germany). Adsorption efficiency, *R*%, and its capacity, *q* (mg/g), were determined by using Eqs. (1) and (2).

$$R\% = \frac{C_0 - C_e}{C_0} \times 100 \quad (1)$$

$$q = \frac{C_0 - C_e}{m} \times v \quad (2)$$

where *C*₀ and *C*_{*e*} is initial and final Cd²⁺ concentration (mg/L), *m* is mass of nanocomposite in solution (g), and *v* is volume of experiment solution (L).

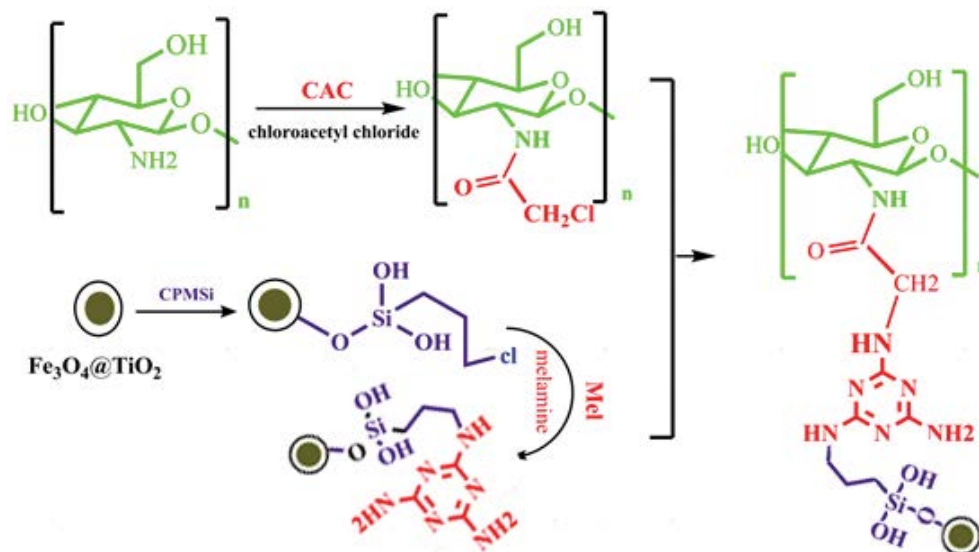
3. Results and discussion

This study was performed on the basis of presenting new bio-based composite which can be incorporated in water

purification industry. Chitosan as one of the promising and reliable biostructures has been employed and modification of the structure using magnetic nanoparticles has been done. The whole procedures as depicted in Scheme 1 were done using common synthetic methods and explained in details previously. To evaluate the synthesized structure and survey on its capability in removal of pollutants, at first, spectral and thermophysical characterizations were performed. Then, cadmium ion as one of the hazardous ions which can cause certain environmental difficulties was chosen and efficiency of the adsorbent in removal process was evaluated.

3.1. FT-IR analysis

To search for the possible functional groups and approve the chemical structure of the prepared biocomposite, FT-IR spectra of Fe₃O₄@TiO₂, Fe₃O₄@TiO₂-CPMSi-Mel, Mel, CACS, and Fe₃O₄@TiO₂-CPMSi-Mel-CACS were analyzed. Stretching vibrations at the range of 500–750 cm⁻¹ in Fig. 1(a) are related to Fe-O and Ti-O [28–30]. The presence of OH groups on the surface of nanoparticles was confirmed by peaks at 3,288 and 1,616 cm⁻¹ due to stretching and bending vibration, respectively. Introduction of CPMSi and Mel to the surface of Fe₃O₄@TiO₂ can be confirmed by such peaks for stretching vibration of Si-O group at 1,027 cm⁻¹, bending vibration of CH₂ at 1,438 cm⁻¹, and bands at 2,800–3,000 cm⁻¹ and 1,265 cm⁻¹ represent stretching vibration of C-H₂ and -CH₂Cl groups of CPMSi, respectively (Fig. 1(b)). Stretching bands of hydroxyl group is overlapped with -NH₂ group of Mel at 3,118–3,325 cm⁻¹ [31,32]. Also peaks at 1,154, 1,544, and 1,641 cm⁻¹ correspond to -C-N stretching absorption, -NH bending, and C=N stretching vibrations, respectively. In Fig. 1(c), for Mel, spectral modes of -NH stretching, -NH bending, C=N stretching, CN bending, and deformation of -NH are assigned as peaks at 3,300–3,450, 1,420–1,550, 1,650, 1,180, and 811 cm⁻¹, respectively. FT-IR spectrum of CACS (Fig. 1(d)) shows a broadened stretching band for



Scheme 1. Represents the synthetic pathway to Fe₃O₄@TiO₂-CPMSi-Mel-CACS.

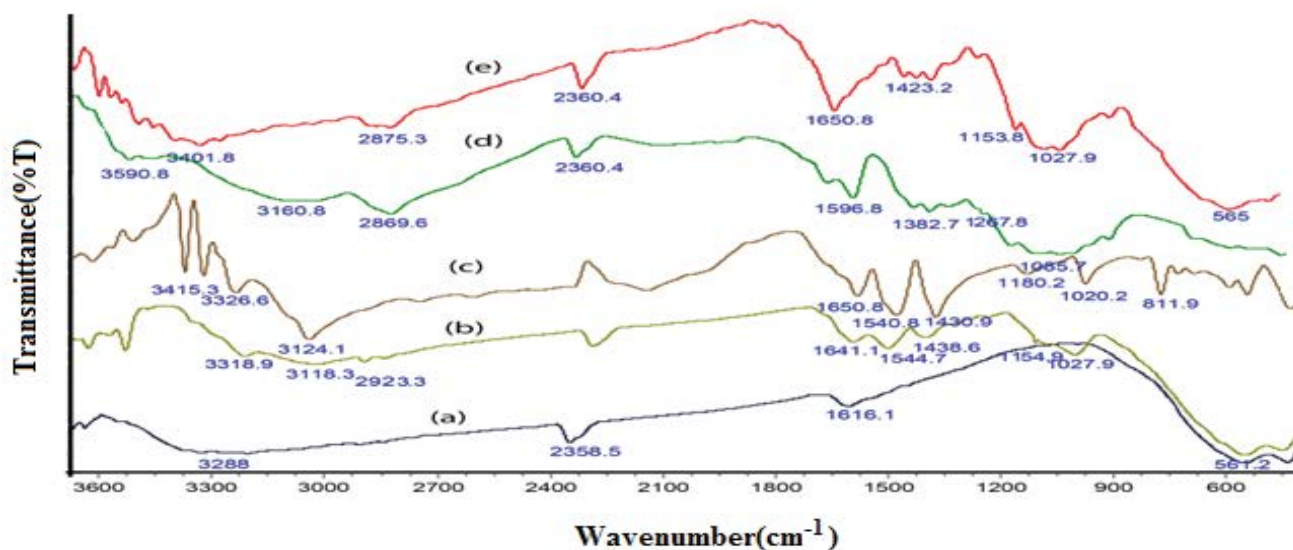


Fig. 1. FT-IR spectra of (a) $\text{Fe}_3\text{O}_4/\text{TiO}_2$, (b) $\text{Fe}_3\text{O}_4/\text{TiO}_2$ -CPMSi-Mel, (c) Melamine, (d) CACS, and (e) $\text{Fe}_3\text{O}_4/\text{TiO}_2$ -CPMSi-Mel-CACS (composite).

OH and NH at $3,000\text{--}3,500\text{ cm}^{-1}$, stretching band of C–H at $2,800\text{--}3,000\text{ cm}^{-1}$, and bands at $1,650$ and $1,596\text{ cm}^{-1}$ referring to *N*-chloroacetyl group in the structure [33]. The IR spectrum of the nanocomposite (Fig. 1(e)) shows all the expected vibrations. The bands at $3,400$ and $3,500\text{ cm}^{-1}$ are related to the OH and NH groups of chitosan and melamine. Peak at $2,875\text{ cm}^{-1}$ is due to –CH stretching vibration and the bands at $1,650$, $1,423$, $1,153.8$, $1,027.9$, and 565 cm^{-1} are attributed to the amide *N*-chloroacetyl, NH bending, C–N bending, Si–O–Si, and Fe–O vibration, respectively, which are approving the presence of functional groups and suggesting the formation of the nanocomposite.

3.2. XRD patterns

The crystallographic structure of nanocomposite was determined by XRD technique. Fig. 2 demonstrates the XRD patterns of the $\text{Fe}_3\text{O}_4/\text{TiO}_2$ (a), $\text{Fe}_3\text{O}_4/\text{TiO}_2$ -CPMSi-Mel (b), and $\text{Fe}_3\text{O}_4/\text{TiO}_2$ -CPMSi-Mel-CACS (c) nanoparticles. In pattern (a), the anatase phase of TiO_2 was detected by its characteristic reflections at about $2\theta = 25.30^\circ$, 48.15° , 54.31° , and 63.05° are indexed to (101), (200), (105), and (204), respectively. In addition, reflections at $2\theta = 38.01^\circ$, 54.31° , and 63.03° are associated with the (311), (422), and (420), respectively, crystalline planes of Fe_3O_4 [34–39]. A similar pattern was observed for $\text{Fe}_3\text{O}_4/\text{TiO}_2$ -CPMSi-Mel as (b), indicating no change in the crystalline $\text{Fe}_3\text{O}_4/\text{TiO}_2$ upon functionalization with 3-chloropropyltrimethoxysilane and melamine. Finally, pattern (c) shows an additional reflection at $2\theta = 20^\circ$ is indexed (110), indicating the occurrence of amorphous chitosan within composite structure [40].

3.3. FESEM and TEM images

The morphology, average size, and distribution of nanoparticles were analyzed by FESEM. Images for $\text{Fe}_3\text{O}_4/\text{TiO}_2$, $\text{Fe}_3\text{O}_4/\text{TiO}_2$ -CPMSi-Mel, $\text{Fe}_3\text{O}_4/\text{TiO}_2$ -CPMSi-Mel-CACS (nanocomposite) and the prepared nanocomposite after Cd^{2+}

adsorption are shown in Fig. 3. Fig. 3(a) shows spherical shape of nanoparticles of $\text{Fe}_3\text{O}_4/\text{TiO}_2$ with an average particle size of $25\text{--}27\text{ nm}$. Fig. 3(b) demonstrates the synthesis of $\text{Fe}_3\text{O}_4/\text{TiO}_2$ -CPMSi-Mel with particles size in the range of $35\text{--}37\text{ nm}$, which were approved by TEM images. Fig. 3(c) shows the final nanocomposite and Fig. 3(d) displays the morphology of the surface of nanocomposite after adsorption.

TEM images of $\text{Fe}_3\text{O}_4/\text{TiO}_2$ -CPMSi-Mel-CACS nanocomposite in 50 and 100 nm scales are depicted in Fig. 4. Dark sections are attributed to $\text{Fe}_3\text{O}_4/\text{TiO}_2$ nanoparticles with average size in the range of $33\text{--}37\text{ nm}$.

3.4. Thermal analysis

Thermal stability of nanoparticles by measuring the amount of weight changes as a function of increasing temperature over period of time was studied by TGA analysis. The obtained curves for synthesized compounds $\text{Fe}_3\text{O}_4/\text{TiO}_2$, $\text{Fe}_3\text{O}_4/\text{TiO}_2$ -CPMSi-Mel, and $\text{Fe}_3\text{O}_4/\text{TiO}_2$ -CPMSi-Mel-CACS are shown in Fig. 5. The result for $\text{Fe}_3\text{O}_4/\text{TiO}_2$ shows that nanoparticles were stable over the studied temperature ranging from 25°C up to 900°C . As can be seen in Fig. 5(b), predictable weight loss due to the decomposition of small organic parts around $130^\circ\text{C}\text{--}250^\circ\text{C}$ is clear. In comparison, different pattern was obtained for $\text{Fe}_3\text{O}_4/\text{TiO}_2$ -CPMSi-Mel-CACS in Fig. 5(c). The main weight losses are attributed to the thermal decomposition of organic components originated from Mel and CACS [41–43].

3.5. CHN analysis

Table 1 summarizes the results of CHN elemental analysis for chitosan, CACS, $\text{Fe}_3\text{O}_4/\text{TiO}_2$, $\text{Fe}_3\text{O}_4/\text{TiO}_2$ -CPMSi, $\text{Fe}_3\text{O}_4/\text{TiO}_2$ -CPMSi-Mel, and $\text{Fe}_3\text{O}_4/\text{TiO}_2$ -CPMSi-Mel-CACS. These results confirm that Mel and CPMSi were incorporated onto backbone of chitosan, in good agreement with literature [44,45]. Presence of functional groups such as amine groups or nitrogen-rich compounds in the composite

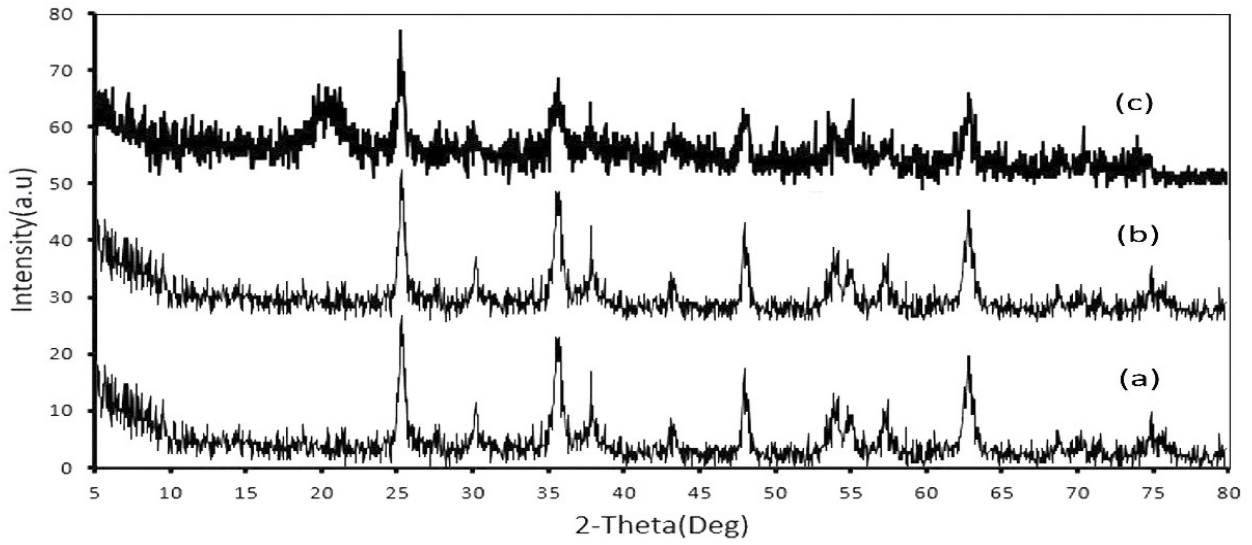


Fig. 2. XRD patterns of $\text{Fe}_3\text{O}_4@TiO_2$ (a), $\text{Fe}_3\text{O}_4@TiO_2\text{-CPMSi-Mel}$ (b), and $\text{Fe}_3\text{O}_4@TiO_2\text{-CPMSi-Mel-CACS}$ composite (c).

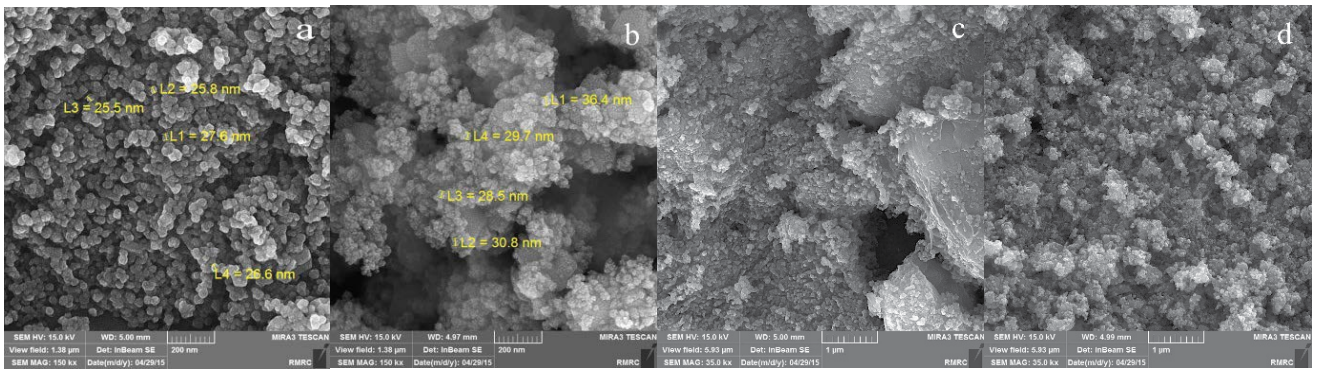


Fig. 3. FESEM image of $\text{Fe}_3\text{O}_4@TiO_2$ (a), $\text{Fe}_3\text{O}_4@TiO_2\text{-CPMSi-Mel}$ (b), $\text{Fe}_3\text{O}_4@TiO_2\text{-CPMSi-Mel-CACS}$ (nanocomposite) (c), and nanocomposite after Cd^{2+} adsorption (d).

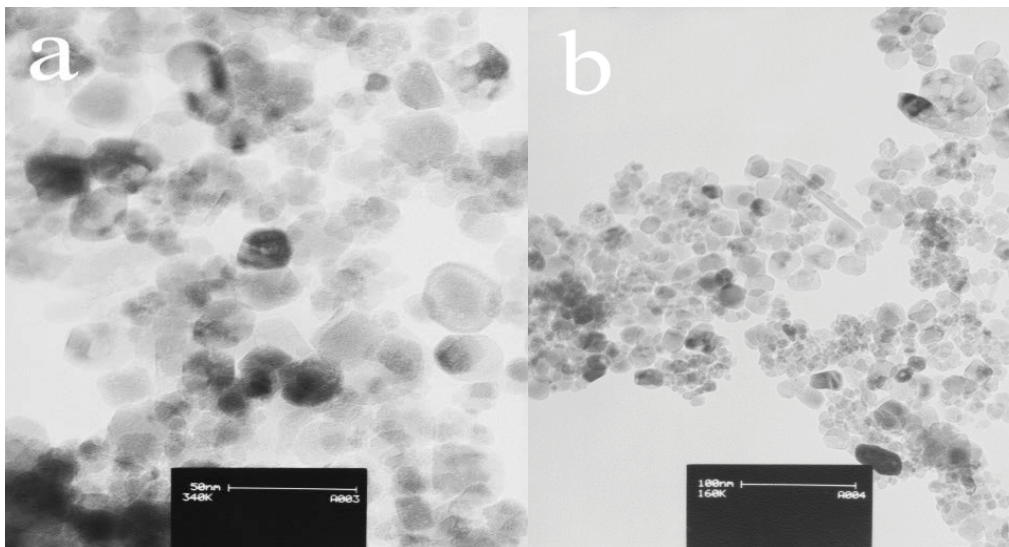


Fig. 4. TEM image of $\text{Fe}_3\text{O}_4@TiO_2\text{-CPMSi-Mel-CACS}$, (a) (50 nm) and (b) (100 nm).

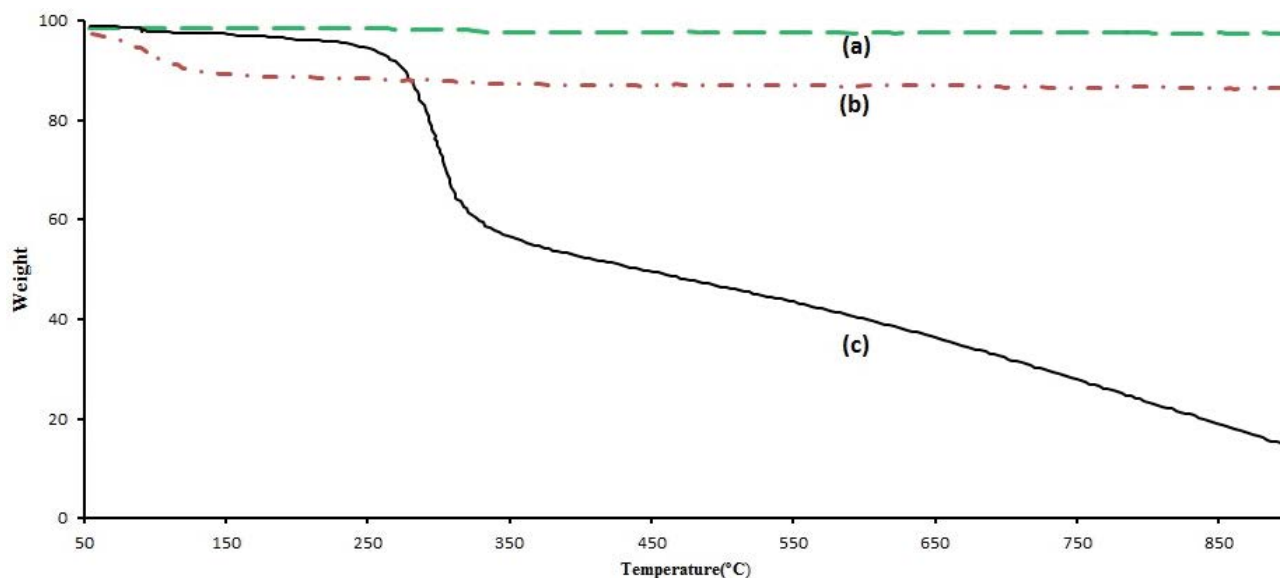


Fig. 5. TGA of $\text{Fe}_3\text{O}_4/\text{TiO}_2$ (a), $\text{Fe}_3\text{O}_4/\text{TiO}_2$ -CPMSi-Mel (b), and $\text{Fe}_3\text{O}_4/\text{TiO}_2$ -CPMSi-Mel-CACS (c).

Table 1
CHN elemental analysis

| Sample | %C | %N | %H |
|------------------------------------------------------|-------|-------|------|
| Chitosan | 39.66 | 6.58 | 6.01 |
| CACS | 41.67 | 7.01 | 6.95 |
| $\text{Fe}_3\text{O}_4/\text{TiO}_2$ | – | – | – |
| $\text{Fe}_3\text{O}_4/\text{TiO}_2$ -CPMSi | 2.93 | – | 0.01 |
| $\text{Fe}_3\text{O}_4/\text{TiO}_2$ -CPMSi-Mel | 6.76 | 6.60 | 0.70 |
| $\text{Fe}_3\text{O}_4/\text{TiO}_2$ -CPMSi-Mel-CACS | 50.26 | 12.04 | 7.62 |

structure will enhance the adsorption capacity due to the greater interaction between metal ion and the mentioned functional groups.

3.6. Magnetization of nanoparticles

Magnetization curves of $\text{Fe}_3\text{O}_4/\text{TiO}_2$, $\text{Fe}_3\text{O}_4/\text{TiO}_2$ -CPMSi-Mel, and $\text{Fe}_3\text{O}_4/\text{TiO}_2$ -CPMSi-Mel-CACS were obtained by VSM at room temperature, and depicted in Fig. 6. According to the result, the saturation magnetization values of 28.97 (emu/g) and 8,500.43 Oe for $\text{Fe}_3\text{O}_4/\text{TiO}_2$, 27.87 (emu/g) and 8,436.04 Oe for $\text{Fe}_3\text{O}_4/\text{TiO}_2$ -CPMSi-Mel and 3.29 (emu/g) and 8,501.08 Oe for $\text{Fe}_3\text{O}_4/\text{TiO}_2$ -CPMSi-Mel-CACS were obtained. A slight reduction of saturation magnetization was observed when CPMSi and Mel were immobilized on the surface of $\text{Fe}_3\text{O}_4/\text{TiO}_2$. In contrast, $\text{Fe}_3\text{O}_4/\text{TiO}_2$ -CPMSi-Mel-CACS exhibits a high decrease in magnetization, which could be due to CACS layers surrounding the nanoparticles [46]. The separation efficiency of $\text{Fe}_3\text{O}_4/\text{TiO}_2$ -CPMSi-Mel-CACS from water by low magnetic field is shown in Fig. 6(B). As shown, in the absence of any magnetic field, it takes about 20 min for the sedimentation of nanocomposite. While, under a low magnetic field (<0.045 T), the sedimentation time decreases by 120-folds. Fast and simple magnetic separation of nanocomposite from solutions makes them an efficient adsorbent for treatments of polluted water.

3.7. Adsorption studies

3.7.1. Effect of pH

The pH factor is an essential element affecting the efficient elimination of ions from aqueous solutions. Dependence of metal ion adsorption to the pH factor can largely be related to the type and the ionic state of functional groups existing in the adsorbent surface as well as metal chemistry in solution. So, to explain this effect, Cd(II) adsorption was examined at pH values of 3, 5, 6, 7, 9, and 10. Fig. 7 shows that removal percentages are enhanced by increasing pH, and by passing through an inflection point around pH = 6 reaches to high values in alkaline conditions. The effect of pH can also be explained by pH_{zpc} of the adsorbent. According to our supplementary experiments the pH_{zpc} of the prepared nanocomposite was found to be 5.2. By regarding the structure of the product, when the pH of the adsorbate solution is lower than the pH_{zpc} , the surface charge of the adsorbent will be positive, while it will be negative at a pH above the pH_{zpc} . Thus, in acidic condition, the effect of protons is predominant so as a result the amine groups are protonated and the surface of the adsorbent is positively charged. Due to the existence of repulsion forces, the availability of surface to adsorb positive metal ions is decreased and leads to a less adsorption capacity so the uptake of Cd^{2+} will be low. However, once the pH of the adsorbate solution is higher than pH_{zpc} , the surface would be negatively charged and will lead to the electrostatic attraction between metal ion and adsorbents surface, resulting in higher adsorption of Cd^{2+} . Moreover, at higher pH, the concentration of Cd^{2+} decreases because of the formation of low soluble hydrolysis species. Therefore, this study was performed at optimum pH = 6. [31,47]

3.7.2. Effect of adsorbent dosage

The removal efficiency of Cd^{2+} was studied in the dosage range of 5–100 mg of adsorbent in 50 mL of Cd^{2+} solutions (50 mg/L). As evident in Fig. 8, the removal percentage

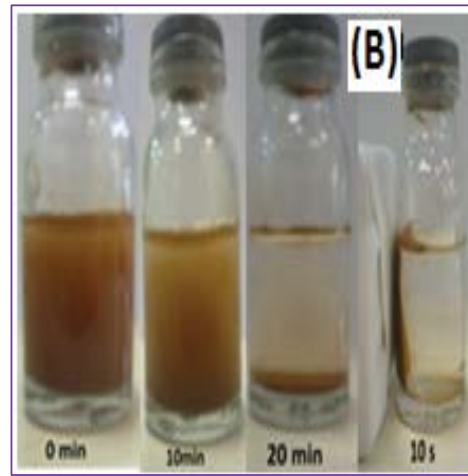
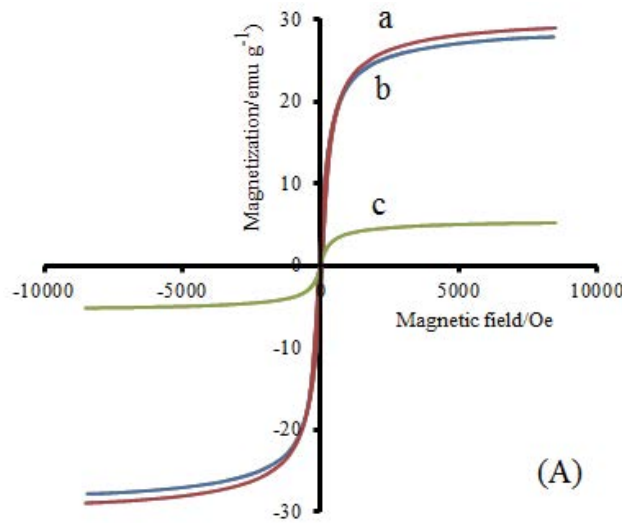


Fig. 6. (A) Magnetization curves of $\text{Fe}_3\text{O}_4@TiO_2$ (a), $\text{Fe}_3\text{O}_4@TiO_2\text{-CPMSi-Mel}$ (b), and nanocomposite (c), (B) sedimentation of nanocomposite from water in the absence (first three samples) and presence of low magnetic field (last sample).

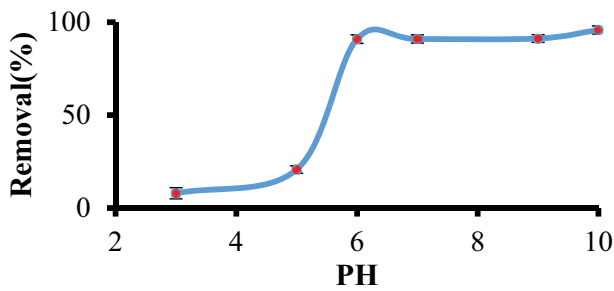


Fig. 7. Effect of pH on the adsorption of Cd^{2+} onto $\text{Fe}_3\text{O}_4@TiO_2\text{-CPMSi-Mel-CACS}$ at 30°C .

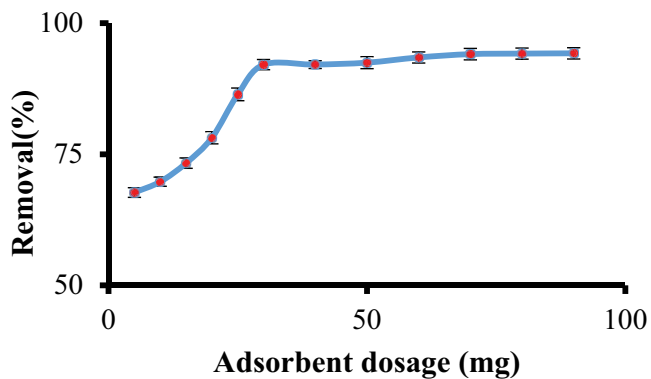


Fig. 8. Effect of adsorbent dosage of $\text{Fe}_3\text{O}_4@TiO_2\text{-CPMSi-Mel-CACS}$ on adsorption of Cd^{2+} at 30°C .

increases sharply up to adsorbent dosage of 30 mg, and then remains approximately constant. This increase in the adsorption is for the reason that more binding sites are accessible on the surface of adsorbent to form complexes with metal ions as the amount of the adsorbent increases. Accordingly, all the

subsequent adsorption studies were performed in solutions with the optimum dosage of adsorbent (30 mg).

3.7.3. Influence of contact time

Fig. 9 represents the results of adsorption dependency to the contact time which was investigated for a 50 mL of 50 mg/L Cd^{2+} solution with an adsorbent dosage of 30 mg at pH of 6.0. As is clear, the removal efficiency increases rapidly with increasing contact time, and reaches finally to an equilibrium state within about 40 min. The metal sorption versus time increases with saturation, suggesting that the possibility of monolayer covering of metal ions on the surface of the adsorbent.

3.7.4. Effect of initial metal Ion concentration on sorption of metal ion

In this study, the experiments were done at different initial concentrations (10–100 mg/L) to determine the effect of initial Cd^{2+} concentration on removal efficiency. Fig. 10 represents results of the adsorption efficiency at optimum conditions (pH = 6, time = 120 min, and adsorbent dosage = 30 mg). The removal of metal ion increases as initial concentration of Cd^{2+} increases from 10 to 40 mg/L, because of the higher collision probability between metal ions and active surface sites resulting in the enhancement of adsorption capacity. With further increases in initial concentration of Cd^{2+} , the removal efficiency decreases due to the saturation of the active surface sites.

3.7.5. Adsorption isotherms studies

In this work, the equilibrium adsorption data were described by well-known adsorption isotherms of Langmuir, Freundlich, and Temkin isotherm models, by which metal ion uptake per mass unit of adsorbent, q_e (mg/g), was related

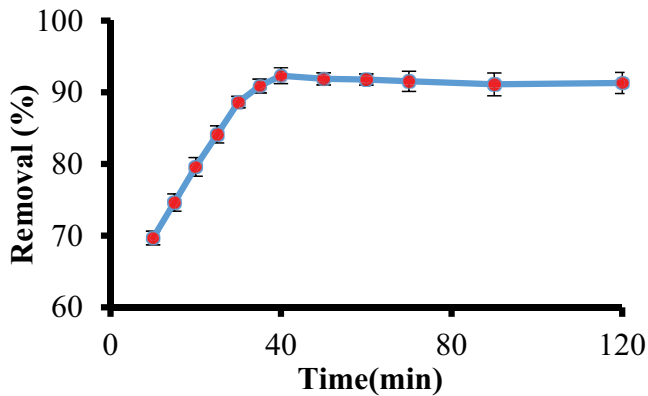


Fig. 9. Effect of contact time on adsorption of Cd^{2+} on $\text{Fe}_3\text{O}_4@$ TiO_2 -CPMSi-Mel-CACS at 30°C .

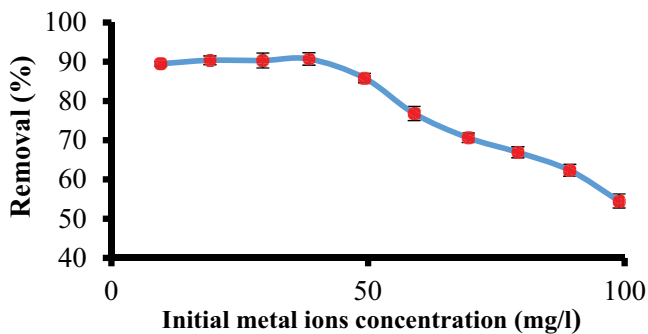


Fig. 10. Effect of initial concentration of Cd^{2+} on its adsorption onto $\text{Fe}_3\text{O}_4@$ TiO_2 -CPMSi-Mel-CACS at 30°C .

to the adsorption equilibrium concentration of metal ion, C_e (mg/L). The linear form of Langmuir, Freundlich, and Temkin isotherm are given by Eqs. (3), (4) and (5), respectively [48–51].

$$\frac{C_e}{q_e} = \frac{1}{q_{\max}b} + \frac{C_e}{q_{\max}} \quad (3)$$

$$\log(q_e) = \log(K_f) + \left(\frac{1}{n}\right)\log(C_e) \quad (4)$$

$$q_e = B \ln A + B \ln C_e \quad (5)$$

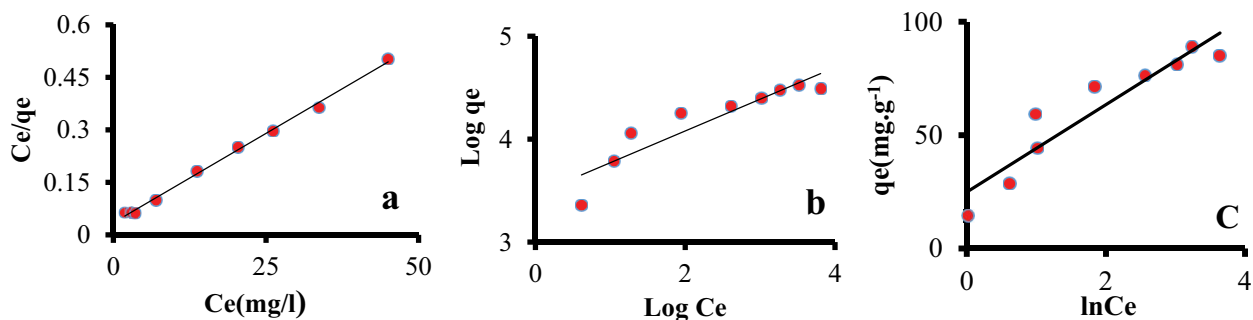


Fig. 11. Langmuir (a), Freundlich (b), and Temkin (c) adsorption isotherms models for adsorption of Cd^{2+} on $\text{Fe}_3\text{O}_4@$ TiO_2 -CPMSi-Mel-CACS ($T = 30^\circ\text{C}$; contact time = 120 min; initial Cd^{2+} concentration = 40 mg/L; adsorbent dosage = 30 mg; pH = 6).

where q_{\max} (mg/g) is the maximum adsorption capacity and b (L/mg) is the Langmuir constant. k_f and n are the Freundlich constants, $B = RT/b_T$ corresponds to the heat of adsorption, where R , T (K), and b_T (J/mol) are the ideal gas constant, the absolute temperature, and Temkin constant, respectively. Temkin isotherm constant A (L/g) is related to the maximum energy of binding. Langmuir model considers the homogeneous surface of adsorbent with the possibility of monolayer adsorption. Whereas Freundlich isotherm assumes the surface heterogeneity in adsorption and the ability to the formation of multilayer during the adsorption. The Temkin isotherm model assumes that the heat of adsorption of all molecules decreases linearly rather than logarithmically with coverage because of the interactions between the adsorbent and adsorbate and the adsorption is characterized by a uniform distribution of binding energies.

Fig. 11 shows the fitted plots of three types of isothermal models. All of the parameters derived from the isothermal models are shown in Table 2 at different temperature. The correlation coefficients indicate that the experimental adsorption data were best fitted by Langmuir model at all three temperatures that indicating monolayer adsorption behavior. The essential features of the Langmuir isotherm can be expressed in terms of a dimensionless constant separation factor (R_L) defined as Eq. (6):

$$R_L = \frac{1}{1 + bC_0} \quad (6)$$

where C_0 (mg/L) is the initial concentration of Cd^{2+} and b is the Langmuir constant. The R_L values between 0 and 1 indicate favorable adsorption for all the initial concentrations and temperatures studied. In this study R_L values were calculated and are given in Table 2. The value within 0.012–0.047 confirms favorable adsorption process for Cd^{2+} ions at all three studied temperatures.

The maximum adsorption capacity, q_{\max} , was 98.03, 99.00, and 101.01 mg/g at 303, 313, and 323 K, respectively. As shown in Table 3, this result is highly comparable with the adsorption capacity of some other modified chitosan-based adsorbent.

3.7.6. Adsorption kinetics

The adsorption mechanism was investigated by examination of pseudo-first-order and pseudo-second-order kinetic models on experimental adsorption data. The equation of

Table 2
Isothermal model parameters derived for adsorption of Cd²⁺ ion on Fe₃O₄@TiO₂-CPMSi-Mel-CACS

| Isotherm model | Parameters | Temperature (K) | | |
|----------------|---------------|-----------------|-------|--------|
| | | 303 | 313 | 323 |
| Langmuir | q_m (mg/g) | 98.03 | 99.00 | 101.01 |
| | b (L/g) | 0.29 | 0.26 | 0.24 |
| | r^2 | 0.99 | 0.98 | 0.99 |
| | R_L | 0.012 | 0.012 | 0.047 |
| Freundlich | n | 3.24 | 3.53 | 3.71 |
| | k_f (mg/g) | 29.96 | 33.11 | 35.51 |
| | $(L/g)^{1/n}$ | 0.84 | 0.78 | 0.77 |
| Temkin | r^2 | | | |
| | A (L/g) | 2.61 | 3.63 | 4.01 |
| | B | 21.22 | 19.26 | 18.61 |
| | r^2 | 0.95 | 0.88 | 0.86 |

pseudo-first-order and pseudo-second order model is given as Eqs. (7) and (8), respectively.

$$\ln(q_e - q_t) = \ln q_e - K_1 t \quad (7)$$

$$\frac{t}{q_t} = \frac{1}{k_2 q_e^2} + \frac{t}{q_e} \quad (8)$$

where q_t (mg/g) is the amount of Cd²⁺ ion adsorbed on the surface at time t , k_1 (min⁻¹) and k_2 (g/(mg min)) are the rate constant of pseudo-first-order and pseudo-second-order model, respectively. The plots of these two kinetics models are shown in Fig. 12. The kinetic parameters derived from the fit of experimental data on both kinetics models are listed in Table 4. The pseudo-second-order model gives a higher r^2 than pseudo-first-order model that indicating the adsorption kinetics of Cd²⁺ on nanocomposite is best described by the pseudo-second-order kinetics model.

The adsorption rate is mainly limited by a chemical adsorption process [64]. It is reasonable because the chelating species exchange process that is mainly a second-order chemical reaction takes places with a much slower rate than the common exchange process controlled mainly by diffusion. Moreover, since there are several chelating groups on the composite surface, it may act as a chelating exchanger in adsorption process. Therefore, it is expected that the chemical complexation reaction occurs during adsorption of Cd²⁺ on the studied adsorbent [65].

3.7.7. Adsorption thermodynamics

The change of Gibbs free energy (ΔG°), enthalpy (ΔH°), and entropy (ΔS°) of adsorption were calculated by Eqs. (9) and (10) to evaluate the thermodynamics behavior of Cd²⁺ ion adsorption onto Fe₃O₄@TiO₂-CPMSi-Mel-CACS [66].

$$\Delta G^\circ = -RT \ln K^\circ \quad (9)$$

$$\ln K^\circ = \frac{\Delta S^\circ}{R} - \frac{\Delta H^\circ}{RT} \quad (10)$$

Thermodynamics adsorption equilibrium constant, K° , was determined at each temperature by plotting q_e/C_e against C_e and then finding extrapolated value at $C_e = 0$. Accordingly, the values of ΔH° and entropy ΔS° were determined by plotting $\ln K^\circ$ versus $1/T$. The results are shown in Table 5. The negative value of ΔG° indicates that adsorption of Cd²⁺ ion adsorption onto Fe₃O₄@TiO₂-CPMSi-Mel-CACS is favorable and takes place spontaneously under the studied conditions. In addition, ΔG° decreases by increasing temperature, indicating the adsorption is a favorable process at higher temperatures. The ΔH° value is negative, indicating the adsorption of Cd²⁺ ion adsorption onto Fe₃O₄@TiO₂-CPMSi-Mel-CACS is an exothermic process. The positive ΔS° value reveals that the randomness increases upon adsorption on the adsorbent surface, which may be due to solvent-adsorbate molecules displacement and adsorbent-adsorbate complex rearrangement.

Table 3
Adsorption capacity (mg/g) of some modified chitosan nanocomposite for Cd²⁺ adsorption

| Adsorbent | Adsorption capacity (mg/g) | Reference |
|----------------------------------------------------------------------|----------------------------|-----------|
| Nanoparticle (Fe ₃ O ₄ /TiO ₂) | (101,12.2) | [52] |
| Chitosan/activated carbon composite | 52.63 | [53] |
| Chitosan nanofibrils | 60.9 | [54] |
| Chitosan biopolymer | 38.5 | [55] |
| Ca(II) imprinted chitosan microspheres | 50.89 | [56] |
| Chitosan-MAA nanoparticles | 1.84 | [57] |
| Magnetic chitosan-2-aminopyridine | 84 | [58] |
| Surfactant-modified chitosan | 125 | [59] |
| Chitosan-based composite | 87.72 | [60] |
| Chitosan pyruvic acid derivative | 98.04 | [61] |
| Chitosan crosslinked with epichlorohydrin-triophosphate | 83.75 | [62] |
| Chitosan microspheres containing 8-hydroxyquinoline -5 sulfonic acid | 32.9 | [63] |

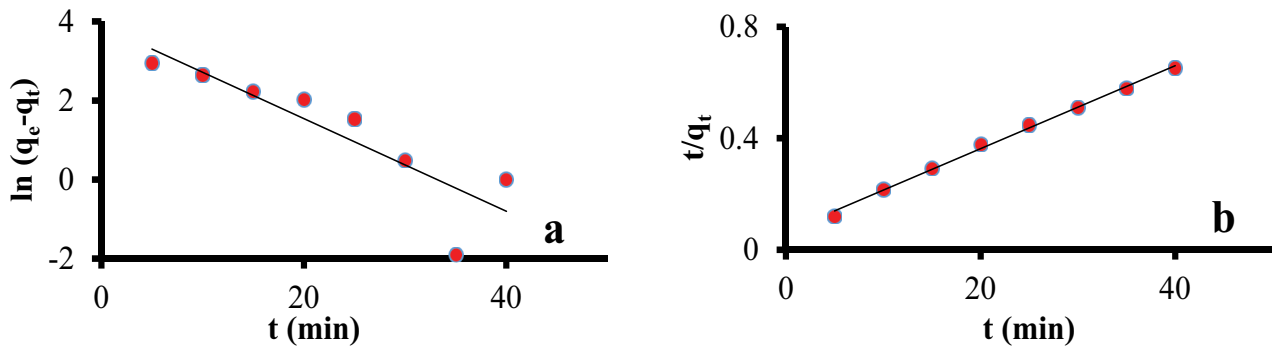


Fig. 12. The plot of (a) pseudo-first-order model and (b) pseudo-second-order model for the adsorption kinetics of Cd^{2+} ion on $\text{Fe}_3\text{O}_4@ \text{TiO}_2\text{-CPMSi-Mel-CACS}$ ($T = 30^\circ\text{C}$; initial Cd^{2+} concentration = 50 mg/L; adsorbent dosage = 30 mg; pH = 6).

Table 4
Kinetic parameters for Cd^{2+} adsorption on $\text{Fe}_3\text{O}_4@ \text{TiO}_2\text{-CPMSi-Mel-CACS}$

| Kinetics model | Parameters | Temperature (K) | | |
|---------------------|--------------------------------------|-----------------|-------|-------|
| | | 303 | 313 | 323 |
| Pseudo-first-order | q_e (mg/g) | 44.70 | 36.59 | 48.42 |
| | k_1 (min^{-1}) | 0.117 | 0.099 | 0.010 |
| | r^2 | 0.77 | 0.96 | 0.86 |
| Pseudo-second-order | q_e (mg/g) | 71.42 | 68.02 | 67.56 |
| | k_2 ($\text{g}/(\text{mg min})$) | 0.003 | 0.002 | 0.003 |
| | r^2 | 0.99 | 0.98 | 0.99 |

Table 5
Thermodynamic parameters for Cd^{2+} adsorption on $\text{Fe}_3\text{O}_4@ \text{TiO}_2\text{-CPMSi-Mel-CACS}$

| Temperature (K) | ΔG° (J/mol) | ΔH° (J/mol) | ΔS° (J/mol K) |
|-----------------|--------------------------|--------------------------|----------------------------|
| 303 | -14,283.24 | -7,679.68 | 21.85 |
| 313 | -14,559.02 | | |
| 323 | -14,779.83 | | |

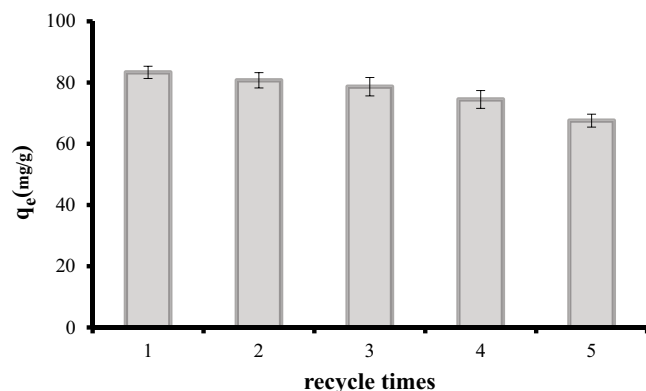


Fig. 13. Cd^{2+} removal efficiency by $\text{Fe}_3\text{O}_4@ \text{TiO}_2\text{-CPMSi-Mel-CACS}$ in five regeneration cycles.

3.7.8. Reusability

Regeneration of an adsorbent for subsequent reuse is an important factor in practical applications. In this work, reusability of adsorbent was evaluated by five times regeneration-adsorption experiments. Regeneration was conducted by transferring 30 mg of Cd^{2+} -loaded adsorbent into 50 mL of 0.01 M HCl and NaHCO_3 and then stirring for 3 h. Thereafter, adsorption experiment was repeated. As shown in Fig. 13, the removal efficiency of regenerated adsorbent was 83.33%, 80.72%, 78.64%, 74.47%, and 67.55% for five consecutive cycles, respectively. This result indicates that $\text{Fe}_3\text{O}_4@ \text{TiO}_2\text{-CPMSi-Mel-CACS}$ has a good reusability and can be used as an efficient adsorbent for Cd^{2+} separation process.

4. Conclusions

The $\text{Fe}_3\text{O}_4@ \text{TiO}_2\text{-CPMSi-Mel-CACS}$ nanocomposite was synthesized successfully via in situ precipitation methods and the sorption experiments showed a high affinity for Cd(II) ion. The reactive inserted functional groups present on the surface of the adsorbents provided more adsorption sites for metal ions. On the other hand, the presence of melamine with nitrogen groups significantly affects nanocomposite sorption capability, and enhanced the adsorption percentage of metal ions. The results disclosed that the highest removal of Cd(II) ions happens in approximately within 40 min at pH 6.0 with 30 mg of adsorbent. The outcomes of

isotherm studies of the Cd(II) metal ion on the Fe₃O₄@TiO₂-CPMSi-Mel-CACS nanocomposite revealed good agreement with the Langmuir models. In addition, this study shows that using melamine moiety in the nanocomposite structure can afford special sorption capacities for removing the other heavy metal ions pollutants. This novel nanocomposite with the mentioned thermophysical and removal capabilities can be regarded as a reliable choice for further industrial and biomedical applications.

References

- [1] F. Fu, Q. Wang, Removal of heavy metal ions from wastewaters: a review, *J. Environ. Manage.*, 92 (2011) 407–418.
- [2] M. Xu, P. Hadi, G. Chen, G. McKay, Removal of cadmium ions from wastewater using innovative electronic waste-derived material, *J. Hazard. Mater.*, 273 (2014) 118–123.
- [3] K. Nogawa, R. Honda, T. Kido, I. Tsuritani, Y. Yamada, M. Ishizaki, H. Yamaya, A dose-response analysis of cadmium in the general environment with special reference to total cadmium intake limit, *Environ. Res.*, 48 (1989) 7–16.
- [4] C.W. Cheung, J.F. Porter, G. McKay, Elovich equation and modified second-order equation for sorption of cadmium ions onto bone char, *J. Chem. Technol. Biotechnol.*, 75 (2000) 963–970.
- [5] Y. Suwazono, E. Kobayashi, Y. Okubo, K. Nogawa, T. Kido, H. Nakagawa, Renal effects of cadmium exposure in cadmium nonpolluted areas in Japan, *Environ. Res.*, 84 (2000) 44–55.
- [6] M.M. Matlock, B.S. Howerton, D.A. Atwood, Chemical precipitation of heavy metals from acid mine drainage, *Water Res.*, 36 (2002) 4757–4764.
- [7] F. Liu, G. Zhang, Q. Meng, H. Zhang, Performance of nanofiltration and reverse osmosis membranes in metal effluent treatment, *Chin. J. Chem. Eng.*, 16 (2008) 441–445.
- [8] Y. Chen, B. Pan, H. Li, W. Zhang, L. Lv, J. Wu, Selective removal of Cu (II) ions by using cation-exchange resin-supported polyethyleneimine (PEI) nanoclusters, *Environ. Sci. Technol.*, 44 (2010) 3508–3513.
- [9] W.M. Golie, S. Upadhyayula, An investigation on biosorption of nitrate from water by chitosan based organic-inorganic hybrid biocomposites, *Int. J. Biol. Macromol.*, 97 (2017) 489–502.
- [10] P. Lodeiro, R. Herrero, M.E. Sastre de Vicente, Thermodynamic and kinetic aspects on the biosorption of cadmium by low cost materials: a review, *Environ. Chem.*, 3 (2006) 400–418.
- [11] S.N. Mohseni, A.A. Amooey, H. Tashakkorian, A. Amouei, A comparative survey of linear and non-linear regression analysis on removal efficiency of clinoptilolite for sorption of dexamethasone from aqueous solutions, *Desal. Wat. Treat.*, 67 (2017) 231–238.
- [12] F. Parhizgar, A. Alishahi, H. Varasteh, H. Rezaee, Removing sodium dodecyl benzene sulfonate (SDBS) from aqueous solutions using chitosan, *J. Polym. Environ.*, 25 (2017) 836–843.
- [13] S. Mallakpour, A. Nezamzadeh Ezeh, Effect of starch-MWCNT@valine nanocomposite on the optical, morphological, thermal, and adsorption properties of chitosan, *J. Polym. Environ.*, 25 (2017) 875–883.
- [14] Q. Liu, Y. Zhao, J. Pan, B. Van der Bruggen, J. Shen, A novel chitosan base molecularly imprinted membrane for selective separation of chlorogenic acid, *Sep. Purif. Technol.*, 164 (2016) 70–80.
- [15] Y.S. Petrova, A.V. Pestov, M.K. Usoltseva, L.K. Neudachina, Selective adsorption of silver (I) ions over copper (II) ions on a sulfoethyl derivative of chitosan, *J. Hazard. Mater.*, 299 (2015) 696–701.
- [16] X. Luo, J. Zeng, S. Liu, L. Zhang, An effective and recyclable adsorbent for the removal of heavy metal ions from aqueous system: magnetic chitosan/cellulose microspheres, *Bioresour. Technol.*, 194 (2015) 403–406.
- [17] H. Jiang, P. Chen, S. Luo, X. Luo, X. Tu, Q. Cao, Y. Zhou, W. Zhang, Synthesis of novel biocompatible composite Fe₃O₄/ZrO₂/chitosan and its application for dye removal, *J. Inorg. Organomet. Polym. Mater.*, 23 (2013) 393–400.
- [18] K. Kalantaria, A.M. Afiffia, A. Salleha, E.N. Mohamada, Z. Izadiyanc, Evaluation of heavy metals removal by cross-linked (polyvinyl alcohol/chitosan/magnetic) nano fibrous membrane prepared by electro spinning technique, *Desal. Wat. Treat.*, 98 (2017) 266–275.
- [19] H.-Y. Zhu, Y.-Q. Fu, R. Jiang, J. Yao, L. Xiao, G.-M. Zeng, Novel magnetic chitosan/poly (vinyl alcohol) hydrogel beads: preparation, characterization and application for adsorption of dye from aqueous solution, *Bioresour. Technol.*, 105 (2012) 24–30.
- [20] A.M. Donia, A.A. Atia, K.Z. Elwakeel, Selective separation of mercury(II) using magnetic chitosan resin modified with Schiff's base derived from thiourea and glutaraldehyde, *J. Hazard. Mater.*, 151 (2008) 372–379.
- [21] Z. Liu, H. Wang, C. Liu, Y. Jiang, G. Yu, X. Mu, X. Wang, Magnetic cellulose–chitosan hydrogels prepared from ionic liquids as reusable adsorbent for removal of heavy metal ions, *Chem. Commun.*, 48 (2012) 7350–7352.
- [22] X.-j. Hu, J.-s. Wang, Y.-g. Liu, X. Li, G.-m. Zeng, Z.-l. Bao, X.-x. Zeng, A.-w. Chen, F. Long, Adsorption of chromium (VI) by ethylenediamine-modified cross-linked magnetic chitosan resin: isotherms, kinetics and thermodynamics, *J. Hazard. Mater.*, 185 (2011) 306–314.
- [23] V. Hasantabar, M. Mansour Lakouraj, H. Tashakkorian, M. Rouhi, Novel nanocomposite based on poly (xanthoneamide-triazole-ethercalix) and TiO₂ nanoparticles: preparation, characterization, and investigation of nanocomposite capability in removal of cationic water pollutants, *Des. Monomers Polym.*, 19 (2016) 607–618.
- [24] S.N. Mohseni, A.A. Amooey, H. Tashakkorian, A.I. Amouei, Removal of dexamethasone from aqueous solutions using modified clinoptilolite zeolite (equilibrium and kinetic), *Int. J. Environ. Sci. Technol.*, 13 (2016) 2261–2268.
- [25] M.M. Lakouraj, H. Tashakkorian, Synthesis and investigation of transition metal removing of novel thermally stable polyamides bearing calix [4] arene in their backbones, *J. Macromol. Sci., Part A*, 49 (2012) 806–813.
- [26] J. Holappa, T. Nevalainen, P. Soininen, M. Elomaa, R. Safin, M. Mässon, T. Järvinen, N-chloroacyl-6-O-triphenylmethylchitosans: useful intermediates for synthetic modifications of chitosan, *Biomacromolecules*, 6 (2005) 858–863.
- [27] Z. Bo, J. Xing, Y. Lang, H. Liu, Synthesis of amino-silane modified magnetic silica adsorbents and application for adsorption of flavonoids from *Glycyrrhiza uralensis* Fisch, *Sci. China, Ser. B*, 51 (2008) 145–151.
- [28] X. Zhang, H. Wang, C. Yang, D. Du, Y. Lin, Preparation, characterization of Fe₃O₄ at TiO₂ magnetic nanoparticles and their application for immunoassay of biomarker of exposure to organophosphorus pesticides, *Biosens. Bioelectron.*, 41 (2013) 669–674.
- [29] Z.-D. Li, H.-L. Wang, X.-N. Wei, X.-Y. Liu, Y.-F. Yang, W.-F. Jiang, Preparation and photocatalytic performance of magnetic Fe₃O₄@TiO₂ core-shell microspheres supported by silica aerogels from industrial fly ash, *J. Alloys Compd.*, 659 (2016) 240–247.
- [30] H. Wang, H.-L. Wang, W.-F. Jiang, Z.-Q. Li, Photocatalytic degradation of 2,4-dinitrophenol (DNP) by multi-walled carbon nanotubes (MWCNTs)/TiO₂ composite in aqueous solution under solar irradiation, *Water Res.*, 43 (2009) 204–210.
- [31] J. Rangel-Mendez, R. Monroy-Zepeda, E. Leyva-Ramos, P. Diaz-Flores, K. Shirai, Chitosan selectivity for removing cadmium (II), copper (II), and lead (II) from aqueous phase: pH and organic matter effect, *J. Hazard. Mater.*, 162 (2009) 503–511.
- [32] M.M.A. Nikje, S.T. Moghaddam, M. Noruzian, M.A.F. Nejad, K. Shabani, M. Haghshenas, S. Shakhshi, Preparation and characterization of flexible polyurethane foam nanocomposites reinforced by magnetic core-shell Fe₃O₄@ APTS nanoparticles, *Colloid. Polym. Sci.*, 292 (2014) 627–633.
- [33] N.G. Kandile, H.M. Mohamed, M.I. Mohamed, New heterocycle modified chitosan adsorbent for metal ions (II) removal from aqueous systems, *Int. J. Biol. Macromol.*, 72 (2015) 110–116.
- [34] E.C.N. Lopes, K.S. Sousa, C. Airoldi, Chitosan–cyanuric chloride intermediary as a source to incorporate molecules – thermodynamic data of copper/biopolymer interactions, *Thermochim. Acta*, 483 (2009) 21–28.

- [35] X. Zhang, H. Wang, C. Yang, D. Du, Y. Lin, Preparation, characterization of Fe_3O_4 at TiO_2 magnetic nanoparticles and their application for immunoassay of biomarker of exposure to organophosphorus pesticides, *Biosens. Bioelectron.*, 41 (2013) 669–674.
- [36] Z. Liu, H. Wang, B. Li, C. Liu, Y. Jiang, G. Yu, X. Mu, Biocompatible magnetic cellulose-chitosan hybrid gel microspheres reconstituted from ionic liquids for enzyme immobilization, *J. Mater. Chem.*, 22 (2012) 15085–15091.
- [37] Z. Lou, Z. Zhou, W. Zhang, X. Zhang, X. Hu, P. Liu, H. Zhang, Magnetized bentonite by Fe_3O_4 nanoparticles treated as adsorbent for methylene blue removal from aqueous solution: synthesis, characterization, mechanism, kinetics and regeneration, *J. Taiwan Inst. Chem. Eng.*, 49 (2015) 199–205.
- [38] Z. Lou, H. Han, M. Zhou, J. Han, J. Cai, C. Huang, J. Zou, X. Zhou, H. Zhou, Z. Sun, Synthesis of magnetic wood with excellent and tunable electromagnetic wave-absorbing properties by a facile vacuum/pressure impregnation method, *ACS Sustain. Chem. Eng.*, 6 (2017) 1000–1008.
- [39] Z. Lou, W. Zhang, X. Hu, H. Zhang, Synthesis of a novel functional group-bridged magnetized bentonite adsorbent: characterization, kinetics, isotherm, thermodynamics and regeneration, *Chin. J. Chem. Eng.*, 25 (2017) 587–594.
- [40] S. Tripathi, G. Mehrotra, P. Dutta, Physicochemical and bioactivity of cross-linked chitosan–PVA film for food packaging applications, *Int. J. Biol. Macromol.*, 45 (2009) 372–376.
- [41] M.A. Zulfikar, S. Afrita, D. Wahyuningrum, M. Ledyastuti, Preparation of Fe_3O_4 -chitosan hybrid nano-particles used for humic acid adsorption, *Environ. Nanotechnol. Monit. Manage.*, 6 (2016) 64–75.
- [42] S. Sobhani, Z.M. Falatoni, M. Honarmand, Synthesis of phosphoric acid supported on magnetic core–shell nanoparticles: a novel recyclable heterogeneous catalyst for Kabachnik–Fields reaction in water, *RSC Adv.*, 4 (2014) 15797–15806.
- [43] R.A. Ahmed, A. Fekry, Preparation and characterization of a nanoparticles modified chitosan sensor and its application for the determination of heavy metals from different aqueous media, *Int. J. Electrochem. Sci.*, 8 (2013) 6692–6708.
- [44] Z.M. dos Santos, A.L.P.F. Caroni, M.R. Pereira, D.R. da Silva, J.L.C. Fonseca, Determination of deacetylation degree of chitosan: a comparison between conductometric titration and CHN elemental analysis, *Carbohydr. Res.*, 344 (2009) 2591–2595.
- [45] O.A.C. Monteiro Jr, C. Airoidi, Some studies of crosslinking chitosan–glutaraldehyde interaction in a homogeneous system, *Int. J. Biol. Macromol.*, 26 (1999) 119–128.
- [46] K. Zargoosh, H. Abedini, A. Abdolmaleki, M.R. Molavian, Effective removal of heavy metal ions from industrial wastes using thiosalicylhydrazide-modified magnetic nanoparticles, *Ind. Eng. Chem. Res.*, 52 (2013) 14944–14954.
- [47] M.E. Mahmoud, M.M. Osman, O.F. Hafez, A.H. Hegazi, E. Elmelegy, Removal and preconcentration of lead (II) and other heavy metals from water by alumina adsorbents developed by surface-adsorbed-dithizone, *Desalination*, 251 (2010) 123–130.
- [48] M. Matouq, N. Jildeh, M. Qtaishat, M. Hindiyeh, M.Q. Al Syouf, The adsorption kinetics and modeling for heavy metals removal from wastewater by *Moringa* pods, *J. Environ. Chem. Eng.*, 3 (2015) 775–784.
- [49] N. Viswanathan, C.S. Sundaram, S. Meenakshi, Development of multifunctional chitosan beads for fluoride removal, *J. Hazard. Mater.*, 167 (2009) 325–331.
- [50] B. González, R. Trujillano, M.A. Vicente, V. Rives, E.H. de Faria, K.J. Ciuffi, S.A. Korili, A. Gil, Doped Ti-pillared clays as effective adsorbents – application to methylene blue and trimethoprim removal, *Environ. Chem.*, 14 (2017) 267–278.
- [51] M. Ghanimati, M. Jabbari, A. Farajtabar, S.A. Nabavi-Amri, Adsorption kinetics and isotherms of bioactive antioxidant quercetin onto amino-functionalized silica nanoparticles in aqueous ethanol solutions, *New J. Chem.*, 41 (2017) 8451–8458.
- [52] A.R. Contreras, A. García, E. Gonzalez, E. Casals, V. Puentes, A. Sanchez, X. Font, S. Recillas, Potential use of CeO_2 , TiO_2 and Fe_3O_4 nanoparticles for the removal of cadmium from water, *Desal. Wat. Treat.*, 41 (2012) 296–300.
- [53] S. Hydari, H. Sharififard, M. Nabavinia, M. Reza Parvizi, A comparative investigation on removal performances of commercial activated carbon, chitosan biosorbent and chitosan/activated carbon composite for cadmium, *Chem. Eng. J.*, 193 (2012) 276–282.
- [54] D. Liu, Z. Li, Y. Zhu, Z. Li, R. Kumar, Recycled chitosan nanofibril as an effective Cu (II), Pb (II) and Cd (II) ionic chelating agent: adsorption and desorption performance, *Carbohydr. Polym.*, 111 (2014) 469–476.
- [55] K.C. Justi, V.T. Fávere, M.C. Laranjeira, A. Neves, R.A. Peralta, Kinetics and equilibrium adsorption of Cu (II), Cd (II), and Ni (II) ions by chitosan functionalized with 2 [bis-(pyridylmethyl) aminomethyl]-4-methyl-6-formylphenol, *J. Colloid Interface Sci.*, 291 (2005) 369–374.
- [56] J. He, Y. Lu, G. Luo, Ca (II) imprinted chitosan microspheres: an effective and green adsorbent for the removal of Cu (II), Cd (II) and Pb (II) from aqueous solutions, *Chem. Eng. J.*, 244 (2014) 202–208.
- [57] A. Heidari, H. Younesi, Z. Mehraban, H. Heikkinen, Selective adsorption of Pb (II), Cd (II), and Ni (II) ions from aqueous solution using chitosan–MAA nanoparticles, *Int. J. Biol. Macromol.*, 61 (2013) 251–263.
- [58] M. Monier, D. Ayad, D. Abdel-Latif, Adsorption of Cu (II), Cd (II) and Ni (II) ions by cross-linked magnetic chitosan-2-aminopyridine glyoxal Schiff's base, *Colloids Surf., B*, 94 (2012) 250–258.
- [59] P. Pal, A. Pal, Surfactant-modified chitosan beads for cadmium ion adsorption, *Int. J. Biol. Macromol.*, 104 (2017) 1548–1555.
- [60] S. Pandey, S. Tiwari, Facile approach to synthesize chitosan based composite – characterization and cadmium (II) ion adsorption studies, *Carbohydr. Polym.*, 134 (2015) 646–656.
- [61] P.O. Boamah, Y. Huang, M. Hua, Q. Zhang, Y. Liu, J. Onumah, W. Wang, Y. Song, Removal of cadmium from aqueous solution using low molecular weight chitosan derivative, *Carbohydr. Polym.*, 122 (2015) 255–264.
- [62] R. Laus, V.T. De Favere, Competitive adsorption of Cu (II) and Cd (II) ions by chitosan crosslinked with epichlorohydrin-triphosphate, *Bioresour. Technol.*, 102 (2011) 8769–8776.
- [63] L. Vitali, M.C.M. Laranjeira, N.S. Gonçalves, V.T. Fávere, Spray-dried chitosan microspheres containing 8-hydroxyquinoline -5 sulphonic acid as a new adsorbent for Cd(II) and Zn(II) ions, *Int. J. Biol. Macromol.*, 42 (2008) 152–157.
- [64] Y.-F. Lin, H.-W. Chen, P.-S. Chien, C.-S. Chiou, C.-C. Liu, Application of bifunctional magnetic adsorbent to adsorb metal cations and anionic dyes in aqueous solution, *J. Hazard. Mater.*, 185 (2011) 1124–1130.
- [65] Y.-T. Zhou, C. Branford-White, H.-L. Nie, L.-M. Zhu, Adsorption mechanism of Cu^{2+} from aqueous solution by chitosan-coated magnetic nanoparticles modified with α -ketoglutaric acid, *Colloids Surf., B*, 74 (2009) 244–252.
- [66] A.A. Khan, R.P. Singh, Adsorption thermodynamics of carbofuran on Sn (IV) arsenosilicate in H^+ , Na^+ and Ca^{2+} forms, *Colloids Surf.*, 24 (1987) 33–42.